

## Unraveling the Interplay of Backbone Rigidity and Electron Rich Side-Chains on Electron Transfer in Peptides: The Realization of Tunable Molecular Wires

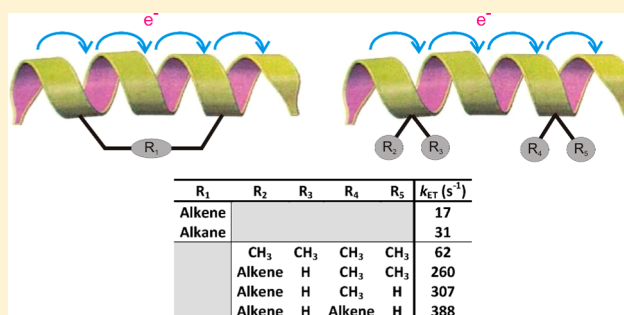
John R. Horsley,<sup>†</sup> Jingxian Yu,<sup>\*,†</sup> Katherine E. Moore,<sup>‡</sup> Joe G. Shapter,<sup>‡</sup> and Andrew D. Abell<sup>\*,†</sup>

<sup>†</sup>ARC Centre of Excellence for Nanoscale BioPhotonics (CNBP), School of Chemistry and Physics, The University of Adelaide, Adelaide, South Australia 5005, Australia

<sup>‡</sup>Centre for Nanoscale Science and Technology, School of Chemical & Physical Science, Flinders University, Bedford Park, South Australia 5042, Australia

### S Supporting Information

**ABSTRACT:** Electrochemical studies are reported on a series of peptides constrained into either a  $3_{10}$ -helix (1–6) or  $\beta$ -strand (7–9) conformation, with variable numbers of electron rich alkene containing side chains. Peptides (1 and 2) and (7 and 8) are further constrained into these geometries with a suitable side chain tether introduced by ring closing metathesis (RCM). Peptides 1, 4 and 5, each containing a single alkene side chain reveal a direct link between backbone rigidity and electron transfer, in isolation from any effects due to the electronic properties of the electron rich side-chains. Further studies on the linear peptides 3–6 confirm the ability of the alkene to facilitate electron transfer through the peptide. A comparison of the electrochemical data for the unsaturated tethered peptides (1 and 7) and saturated tethered peptides (2 and 8) reveals an interplay between backbone rigidity and effects arising from the electron rich alkene side-chains on electron transfer. Theoretical calculations on  $\beta$ -strand models analogous to 7, 8 and 9 provide further insights into the relative roles of backbone rigidity and electron rich side-chains on intramolecular electron transfer. Furthermore, electron population analysis confirms the role of the alkene as a “stepping stone” for electron transfer. These findings provide a new approach for fine-tuning the electronic properties of peptides by controlling backbone rigidity, and through the inclusion of electron rich side-chains. This allows for manipulation of energy barriers and hence conductance in peptides, a crucial step in the design and fabrication of molecular-based electronic devices.



## INTRODUCTION

Electron transfer in proteins plays an important role in a wide range of metabolic processes at the cellular level.<sup>1,2</sup> Many factors have been shown to influence this electron transfer, including the distance separating the electron donor and acceptor,<sup>3–5</sup> the extent of secondary structure,<sup>6,7</sup> dipole moment,<sup>8–10</sup> and the nature of the constituent amino acid side chains.<sup>11–14</sup> Of particular significance is the suggestion that peptides can undergo electron transfer via either a bridge-assisted superexchange or an electron hopping mechanism.<sup>15</sup> While electron superexchange is a one step process that is exponentially dependent on distance, the hopping model involves a multistep process for electron translocations across long distances, whereby the charge temporarily resides on the bridge between redox centers.<sup>16,17</sup> Consequently, electron hopping through a peptide can be facilitated by redox-active amino acid side chains in the sequence that act as “stepping stones” for electron transfer.<sup>18,19</sup> Studies on model peptides have confirmed this, where the rate of electron transfer increases significantly with the introduction of electron rich

side-chains into the peptide.<sup>11</sup> For example, Kimura and co-workers demonstrated that linearly spaced electron rich naphthyl groups within synthetic peptides increase the photocurrent by efficient electron hopping between the moieties, compared to reference peptides containing one or no naphthyl groups.<sup>20</sup> An electron rich tryptophan side chain has also been shown to act as a “relay station” to facilitate multistep electron transfer in an azurin metallo-protein isolated from *Pseudomonas aeruginosa*.<sup>21</sup> Multiple sequence alignment of genomes from the respiratory oxidoreductase enzyme NDH1, have revealed the conservation of specific aromatic amino acids from simple prokaryotes through to man, that may serve as candidates for transient charge localization between metal clusters.<sup>22</sup> The majority of research conducted thus far has focused on aromatic amino acids as the source of electron rich “stepping stones”.

Received: July 15, 2014

Published: August 14, 2014

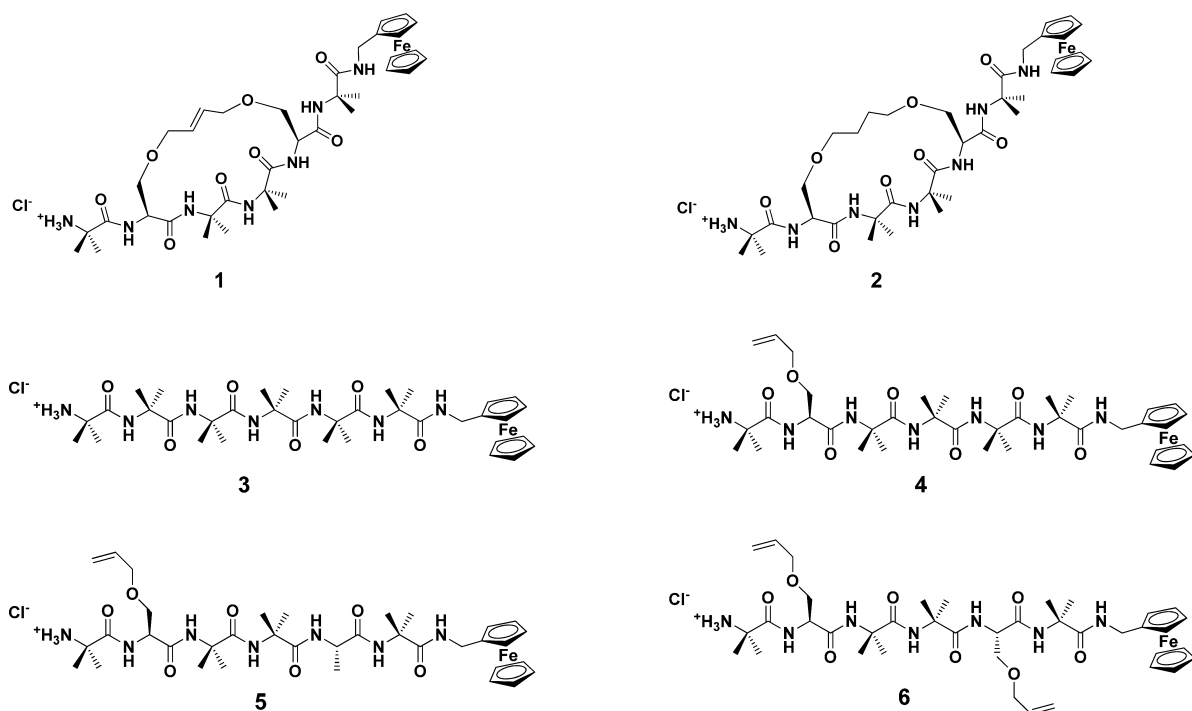


Figure 1. Structures of helical peptides 1–6.

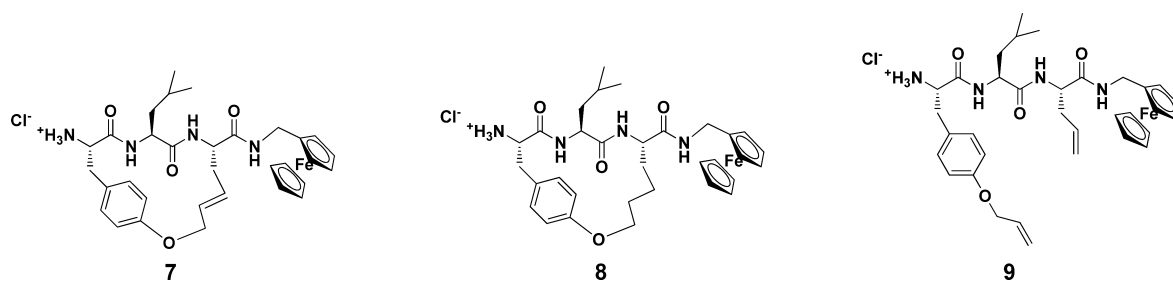


Figure 2. Structures of  $\beta$ -strand peptides 7–9.

Recent work with an Aib ( $\alpha$ -aminoisobutyric acid) rich hexapeptide, constrained into a  $3_{10}$ -helix by a triazole-containing covalent tether linking its  $i$  to  $i + 3$  residues,<sup>23</sup> has shown that backbone rigidity also plays a significant role in defining the rate of electron transfer in peptides. Increased rigidity restricts backbone torsional motion, resulting in an additional reorganization energy barrier to electron transfer. In the study reported here, a series of alkene containing peptides, both linear (see 4, 5, 6, and 9, Figures 1 and 2) and also a series of alkene tethered peptides (see 1 and 7, Figures 1 and 2), is used to begin to unravel the interplay of peptide backbone rigidity and the nature of the amino acid side chains in defining the rate of electron transfer, where until now these effects have been considered without factoring in the other variable. Electrochemical and theoretical studies are presented on peptides constrained into both a  $3_{10}$ -helix (see 1 and 2, Figure 1) and a  $\beta$ -strand (see 7 and 8, Figure 2). The alkene group in the peptides is shown to promote electron transfer, with its influence on backbone rigidity and its role as an electron rich “stepping stone” discussed to explore the generality and connectivity of these effects.

## EXPERIMENTAL METHODS

**Chemicals.** Fmoc-Aib-OH, Boc-Aib-OH, Boc-Ser-OH, Fmoc-OSu, 2-chlorotriyl chloride polystyrene resin, 1-hydroxy-7-azabenzotriazole (HOAt) and 2-(1*H*-7-azabenzotriazol-1-yl)-1,1,3,3-tetramethyl uranium hexafluorophosphate methanaminium (HATU) were purchased from GL Biochem (Shanghai) Ltd., China. Dichloromethane (DCM), diethyl ether (Et<sub>2</sub>O), ethyl acetate (EtOAc), methanol and ethanol were purchased from Ajax Finechem Pty Ltd. (Australia). Piperidine, acetonitrile, propan-2-ol and *N,N*-dimethylformamide (DMF) were purchased from Merck, Australia. Anhydrous *N,N*-dimethylformamide (DMF), dimethyl sulfoxide (DMSO), tetrahydrofuran (THF), Second-generation Grubbs' catalyst, Pd/C catalyst, ethyl vinyl ether, 2,2,2-trifluoroethanol (TFE), trifluoroacetic acid (TFA), 4 M HCl/dioxane solution, *N,N'*-dicyclohexylcarbodiimide (DCC), dimethylaminopyridine (DMAP), cysteamine and diisopropylethylamine (DIPEA) were purchased from Sigma-Aldrich, Australia. NaOH was purchased from Chem Supply, Australia. Single-walled carbon nanotubes (P2-SWCNTs) were purchased from Carbon Solutions, Inc., USA. Boc-Ser(Al)-OH<sup>24</sup> and ferrocenylmethylamine<sup>25,26</sup> were prepared as published. All solvents and reagents were used without purification unless noted.

**High-Performance Liquid Chromatography.** The synthetic peptides were analyzed and purified by reverse phase HPLC, using an HP 1100 LC system equipped with a Phenomenex C18 column (250 × 4.6 mm) for analytical traces and a Phenomenex C18 column (250 × 21.2 mm) for purification, a photodiode array detector, and a Sedex

evaporative light scattering detector. Water/TFA (100/0.1 by v/v) and ACN/TFA (100/0.08 by v/v) solutions were used as aqueous and organic buffers.

**NMR Spectroscopy.**  $^1\text{H}$  NMR spectra were recorded in DMSO- $d_6$  or  $\text{CDCl}_3$ - $d$  solutions using a Varian Gemini-300 NMR.  $^{13}\text{C}$  NMR and two-dimensional NMR experiments utilizing COSY, ROESY, HSQC and HMBC, were obtained on a Varian Inova 600 MHz spectrometer. Chemical shifts are reported in ppm ( $\delta$ ) using TMS (0.00 ppm) as the internal standard. Signals are reported as s (singlet), d (doublet), t (triplet) or m (multiplet).

**Mass Spectroscopy.** Low resolution mass spectral data were analyzed using a Finnigan MAT LCQ spectrometer with MS/MS and ESI probe, utilizing XCalibur software. High resolution mass spectral data were analyzed using an Ultimate 3000 RSL HPLC (Thermo Fisher Scientific Inc., MA) and an LTQ Orbitrap XL ETD using a flow injection method, with a flow rate of 5  $\mu\text{L}/\text{min}$ . The HPLC flow is interfaced with the mass spectrometer using the Electrospray source (Thermo Fisher Scientific Inc., MA). Mass spectra were obtained over a range of  $100 < m/z < 1000$ . Data were analyzed using XCalibur software (Version 2.0.7, Thermo Fisher Scientific).

**FTIR Spectroscopy.** Infrared spectra were collected on a PerkinElmer Spectrum 100 FT-IR spectrometer, with attenuated total reflectance (ATR) imaging capabilities, fitted with a ZnSe crystal, with an average reading taken from 4 scans at 4  $\text{cm}^{-1}$  resolution.

**Peptide Synthesis.** The linear hexapeptides (**3**,<sup>23</sup> **4**, **5** and **6**) were synthesized using solid phase peptide synthesis on 2-chlorotrityl chloride resin using Fmoc-Aib-OH, Fmoc-protected allyl serine, and HATU/DIPEA coupling conditions as detailed in the Supporting Information. Cleavage from the resin was followed by C-terminal coupling with ferrocenylmethylamine, and the N-terminal Boc group was removed to give the free amine for coupling to a single-walled carbon nanotube (SWCNTs)/Au electrode assembly. The  $3_{10}$ -helical (**1**) and  $\beta$ -strand (**7**) macrocycles were prepared by ring closing metathesis of the appropriate dienes as detailed in the Supporting Information. Peptide **1** involves linking the  $i$  to  $i + 3$  residues using a strategy previously reported by O'Leary and co-workers.<sup>24</sup> In this study the geometry of a related sequence was confirmed by X-ray crystallography.<sup>24</sup> For both of these peptides a single alkene isomer was obtained which was assigned the (*E*)-configuration based on the alkene coupling constant<sup>27</sup> (15.8 Hz for **7**). The C-terminal ferrocenyl group and N-terminal free amine were introduced as above. The saturated analogues (**2** and **8**) were prepared by hydrogenation of the macrocyclic alkenes and the linear peptide **9** was prepared by simple peptide coupling in solution. All peptides (**1**–**9**) were purified using reverse phase HPLC prior to attachment to the SWCNTs/Au electrode by HATU/DIPEA.

**General Procedure for N-Boc Cleavage.** The N-Boc protected peptides **1**–**9** were dissolved in trifluoroethanol (TFE), and 4 M HCl in 1,4-dioxane was added. The reaction solution was stirred at rt for 20–30 min, and the solvent removed *in vacuo*.

**Peptide 1.**  $^1\text{H}$  NMR (600 MHz, DMSO- $d_6$ )  $\delta$  8.49 (s, 1H, NH, Aib4), 8.38 (d, 1H, NH,  $J = 7.9$  Hz, residue2), 8.12 (bs, 3H, NH<sub>3</sub>, Aib1), 7.87 (s, 1H, NH, Aib3), 7.72 (s, 1H, NH, Aib6), 7.45 (d, 1H, NH,  $J = 8.2$  Hz, residue 5), 7.20 (br s, 1H, NH, Fc), 5.73–5.61 (m, 2H, CH=CH), 4.55 (td, 1H, CaH,  $J = 8.3, 5.1$  Hz), 4.41 (s, 1H, CaH), 4.20–3.20 (m, 19H, Cp,  $5 \times \text{CH}_2$ ), 1.53–1.32 (m, 24H,  $8 \times \text{CH}_3$ );  $^{13}\text{C}$  NMR (150 MHz, DMSO- $d_6$ )  $\delta$  174.74, 174.27, 173.16, 171.62, 169.67, 168.72, 157.97, 157.75, 131.00, 126.08, 86.45, 69.45, 69.31, 68.31, 68.00, 66.98, 65.88, 56.46, 56.41, 56.37, 56.19, 56.13, 54.78, 52.58, 37.85, 26.11, 26.00, 25.61, 25.34, 24.92, 24.41, 24.30, 23.36, 23.28, 23.22, 23.11; HRMS  $[\text{M}]^+_{\text{calcd}} = 782.34561$ ,  $[\text{M}]^+_{\text{found}} = 782.34567$ .

**Peptide 2.**  $^1\text{H}$  NMR (600 MHz, DMSO- $d_6$ )  $\delta$  8.54 (s, 1H, NH, Aib3), 8.18 (bs, 3H, NH<sub>3</sub>, Aib1), 8.05 (s, 1H, NH, Aib4), 7.62 (s, 1H, NH, Aib6), 7.57 (d, 1H, NH,  $J = 6.4$  Hz, residue2), 7.34 (d, 1H, NH,  $J = 6.7$  Hz, residue5), 7.26 (t, 1H, NH (Fc),  $J = 5.8$  Hz), 4.42 (m, 1H, CaH), 4.14 (m, 1H, CaH), 4.20–3.30 (m, 19H, Cp,  $2 \times \text{CaHCH}_2$ ,  $3 \times \text{CH}_2$ ), 1.73–1.33 (m, 28H,  $2 \times \text{CH}_2$ ,  $8 \times \text{CH}_3$ );  $^{13}\text{C}$  NMR (150 MHz, DMSO- $d_6$ )  $\delta$  175.14, 174.58, 173.33, 171.20, 169.38, 168.87, 86.45, 71.42, 69.40, 69.33, 68.74, 68.55, 68.32, 67.02, 66.96, 66.91,

56.46, 56.34, 56.20, 56.18, 55.90, 55.66, 53.31, 48.56, 37.87, 26.76, 26.46, 26.10, 25.50, 24.35, 24.32, 23.53, 23.50, 23.45, 23.33, 23.21, 23.01; HRMS  $[\text{M}]^+_{\text{calcd}} = 783.36126$ ,  $[\text{M}]^+_{\text{found}} = 783.3611$ .

**Peptide 3.**  $^1\text{H}$  NMR (600 MHz, DMSO- $d_6$ ),  $^{13}\text{C}$  NMR (150 MHz, DMSO- $d_6$ ) as previously reported.<sup>23</sup>

**Peptide 4.**  $^1\text{H}$  NMR (600 MHz, DMSO- $d_6$ )  $\delta$  8.65 (s, 1H, NH), 8.29 (d, 1H, NH,  $J = 7.3$  Hz), 8.12 (br s, 3H, NH<sub>3</sub>), 7.63 (s, 1H, NH), 7.59 (s, 1H, NH), 7.54 (t, 1H, NH,  $J = 6.0$  Hz), 7.38 (s, 1H, NH), 5.90 (ddt, 1H, CH=CH<sub>2</sub>,  $J = 17.1, 10.6, 5.3$  Hz), 5.29 (ddd, 1H, CH=CH<sub>2</sub>,  $J = 17.3, 3.4, 1.6$  Hz), 5.19 (dd, 1H, CH=CH<sub>2</sub>,  $J = 10.5, 1.6$  Hz), 4.56 (dd, 1H, CaH,  $J = 13.0, 7.5$  Hz), 4.22–3.92 (m, 13H, Cp, CH<sub>2</sub>, OCH<sub>2</sub>), 3.79 (dd, 1H, CHCH<sub>2</sub>CO,  $J = 10.1, 5.4$  Hz), 3.64 (dd, 1H, CHCH<sub>2</sub>CO,  $J = 10.1, 8.0$  Hz), 1.50–1.29 (m, 30H,  $10 \times \text{CH}_3$ );  $^{13}\text{C}$  NMR (150 MHz, DMSO- $d_6$ )  $\delta$  174.76, 174.24, 173.80, 173.46, 171.81, 169.70, 134.80, 116.73, 86.73, 71.07, 68.98, 68.79, 68.72, 68.62, 68.35, 66.97, 66.84, 56.34, 56.16, 56.04, 55.99, 55.95, 53.25, 37.78, 28.98, 26.00, 25.36, 25.04, 24.97, 24.79, 24.47, 24.08, 23.46, 23.34; LRMS  $[\text{M}]^+_{\text{calcd}} = 768.3747$ ,  $[\text{M}]^+_{\text{found}} = 768.3764$ .

**Peptide 5.**  $^1\text{H}$  NMR (600 MHz, DMSO- $d_6$ )  $\delta$  8.71 (s, 1H, NH),  $\delta$  8.28 (d, 1H, NH,  $J = 6.9$  Hz),  $\delta$  8.14 (br s, 3H, NH),  $\delta$  7.63–7.58 (m, 3H, NH),  $\delta$  7.31 (br s, 1H, NH),  $\delta$  5.90 (ddd, 1H, OCH<sub>2</sub>CH,  $J = 22.3, 10.5, 5.2$ ),  $\delta$  5.28 (d, 1H, OCH<sub>2</sub>CH,  $J = 17.2$  Hz),  $\delta$  5.18 (d, 1H, OCH<sub>2</sub>CH,  $J = 10.5$  Hz),  $\delta$  4.54 (dd, 1H, CaH,  $J = 13.0, 6.9$  Hz),  $\delta$  4.27–4.08 (m, 9H, Cp), 4.06–3.99 (m, 2H, OCH<sub>2</sub>CH),  $\delta$  3.95–3.87 (m, 2H, CH<sub>2</sub>Fc),  $\delta$  3.90 (m, 1H, CaH),  $\delta$  3.78 (dd, 1H, CaHCH<sub>2</sub>,  $J = 10.0, 5.5$  Hz),  $\delta$  3.63 (m, 1H, CaHCH<sub>2</sub>),  $\delta$  1.48–1.31 (m, 24H,  $8 \times \text{CH}_3$ ),  $\delta$  1.30–1.27 (m, 3H, CH<sub>3</sub> alanine);  $^{13}\text{C}$  NMR (150 MHz, DMSO- $d_6$ )  $\delta$  175.5, 174.5, 172.5, 172.3, 170.3, 135.3, 117.2, 83.4, 71.4, 69.2, 56.8, 56.6, 56.5, 56.3, 53.8, 50.8, 50.3, 26.6, 26.2, 25.5, 25.1, 24.39, 24.30, 23.9, 23.7; HRMS  $[\text{M}]^+_{\text{calcd}} = 754.3585$ ,  $[\text{M}]^+_{\text{found}} = 754.3588$ .

**Peptide 6.**  $^1\text{H}$  NMR (600 MHz, DMSO- $d_6$ )  $\delta$  8.60 (s, 1H, NH), 8.24 (d, 1H, NH,  $J = 6.9$  Hz), 8.12 (s, 3H, NH<sub>3</sub>), 7.73 (s, 1H, NH), 7.60 (d, 1H, NH,  $J = 6.3$  Hz), 7.50 (s, 1H, NH), 7.32 (t, 1H, NH, 5.7 Hz), 5.84 (m, 2H,  $2 \times \text{CH}=\text{CH}_2$ ), 5.30–5.10 (m, 4H,  $2 \times \text{CH}=\text{CH}_2$ ), 4.56 (dd, 1H, CaH,  $J = 13.2, 6.8$  Hz), 4.25–3.60 (m, 20H, Cp, CaH,  $5 \times \text{CH}_2$ ), 1.55–1.25 (m, 24H,  $8 \times \text{CH}_3$ );  $^{13}\text{C}$  NMR (150 MHz, DMSO- $d_6$ )  $\delta$  175.00, 173.94, 173.30, 171.74, 169.57, 169.14, 134.87, 134.74, 116.80, 116.29, 109.51, 86.41, 73.00, 71.07, 70.83, 69.35, 68.83, 68.70, 68.53, 68.30, 68.14, 67.06, 67.02, 66.98, 66.94, 56.36, 56.10, 55.95, 54.54, 53.32, 37.80, 25.66, 25.33, 25.13, 25.01, 24.13, 24.06, 23.46, 23.31; LRMS  $[\text{M}]^+_{\text{calcd}} = 810.3852$ ,  $[\text{M}]^+_{\text{found}} = 810.3834$ .

**Peptide 7.**  $^1\text{H}$  NMR (600 MHz, DMSO- $d_6$ )  $\delta$  8.30 (d, 3H, NH Tyr,  $J = 3.4$  Hz),  $\delta$  8.20 (d, 1H, NH Gly,  $J = 8.7$  Hz),  $\delta$  7.99 (t, 1H, NH Fc,  $J = 5.8$  Hz),  $\delta$  7.93 (d, 1H, NH Leu,  $J = 8.0$  Hz),  $\delta$  6.96 (d, 2H, ArH,  $J = 7.9$  Hz),  $\delta$  6.72 (d, 2H, ArH,  $J = 8.7$  Hz),  $\delta$  5.64–5.60 (dt, 1H, OCH<sub>2</sub>CH,  $J = 15.8, 4.3$  Hz),  $\delta$  5.54–5.50 (m, 1H, OCH<sub>2</sub>CHCH),  $\delta$  4.67–4.60 (m, 2H, OCH<sub>2</sub>CH),  $\delta$  4.41–4.37 (ddd, 1H, CaH Gly,  $J = 11.8, 8.8, 2.7$  Hz),  $\delta$  4.23–4.18 (m, 1H, CaH Tyr),  $\delta$  4.16–4.10 (m, 1H, CaH Leu),  $\delta$  4.16–4.04 (m, 9H, Cp),  $\delta$  4.00–3.91 (ddd, 2H, CH<sub>2</sub>Fc,  $J = 30.9, 14.8, 5.8$  Hz),  $\delta$  3.05–3.02 (dd, 1H, CaHCH<sub>2</sub>Ph,  $J = 13.1, 5.7$  Hz),  $\delta$  2.71–2.67 (dd, 1H, CaHCH<sub>2</sub>Ph,  $J = 12.9, 10.6$  Hz),  $\delta$  2.35 (d, 1H, OCH<sub>2</sub>CHCHCH,  $J = 15.5$  Hz),  $\delta$  2.27–2.21 (m, 1H, OCH<sub>2</sub>CHCHCH),  $\delta$  1.54–1.48 (m, 1H, CaHCH<sub>2</sub>CH(CH<sub>3</sub>)<sub>2</sub>),  $\delta$  1.36–1.27 (m, 2H, CaHCH<sub>2</sub>CH(CH<sub>3</sub>)<sub>2</sub>),  $\delta$  0.84–0.82 (m, 6H, CaHCH<sub>2</sub>CH(CH<sub>3</sub>)<sub>2</sub>);  $^{13}\text{C}$  NMR (150 MHz, DMSO- $d_6$ )  $\delta$  170.5, 166.4, 156.0, 129.8, 129.2, 127.3, 114.9, 86.0, 72.9, 69.4, 69.3, 68.2, 67.3, 67.2, 67.1, 65.8, 52.6, 52.5, 50.8, 43.5, 37.3, 36.0, 33.6, 23.6, 22.8, 22.7; HRMS  $[\text{M} + \text{H}]^+$  calculated for C<sub>32</sub>H<sub>40</sub>FeN<sub>4</sub>O<sub>4</sub>, 600.23916, found 600.23935; IR 1635  $\text{cm}^{-1}$ , 1686  $\text{cm}^{-1}$  (shoulder) (Amide I Band); 1513  $\text{cm}^{-1}$ , 1529  $\text{cm}^{-1}$  (Amide II Band); 3292  $\text{cm}^{-1}$  (Amide A Band).

**Peptide 8.**  $^1\text{H}$  NMR (600 MHz, DMSO- $d_6$ )  $\delta$  8.32 (d, 3H, NH Tyr,  $J = 4.1$  Hz),  $\delta$  8.11 (d, 1H, NH Gly,  $J = 9.1$  Hz),  $\delta$  7.96 (t, 1H, NH Fc,  $J = 5.8$  Hz),  $\delta$  7.80 (d, 1H, NH Leu,  $J = 7.8$  Hz),  $\delta$  7.00 (d, 2H, ArH,  $J = 7.7$  Hz),  $\delta$  6.79 (d, 2H, ArH,  $J = 8.6$  Hz),  $\delta$  4.35–4.25 (m, 3H, OCH<sub>2</sub>CH<sub>2</sub>CH<sub>2</sub>, CaH Gly, CaH Tyr),  $\delta$  4.19–4.01 (m, 11H, Cp, CH<sub>2</sub>), OCH<sub>2</sub>CH<sub>2</sub>CH<sub>2</sub>, CaH Leu),  $\delta$  3.97–3.92 (dd, 2H, CH<sub>2</sub>Fc,  $J = 15.8, 6.1$  Hz),  $\delta$  3.08–3.05 (dd, 1H, CaHCH<sub>2</sub>Ph,  $J = 12.8, 5.8$  Hz),  $\delta$  2.65–2.61 (m, 1H, CaHCH<sub>2</sub>Ph),  $\delta$  1.78–1.70 (m, 1H,

OCH<sub>2</sub>CHHCH<sub>2</sub>),  $\delta$  1.61–1.47 (m, 3H, OCH<sub>2</sub>CH<sub>2</sub>CHHCHH, CaHCH<sub>2</sub>CH(CH<sub>3</sub>)<sub>2</sub>),  $\delta$  1.43–1.21 (m, 5H, OCH<sub>2</sub>CHHCHHCHH, CaHCH<sub>2</sub>CH(CH<sub>3</sub>)<sub>2</sub>),  $\delta$  0.83–0.81 (m, 6H, CaHCH<sub>2</sub>CH(CH<sub>3</sub>)<sub>2</sub>); <sup>13</sup>C NMR (150 MHz, DMSO-*d*<sub>6</sub>)  $\delta$  171.1, 170.2, 166.4, 156.3, 130.1, 126.2, 115.5, 86.1, 73.0, 69.4, 69.3, 68.7, 67.3, 67.2, 67.1, 66.2, 52.6, 50.8, 50.7, 43.6, 40.0, 37.3, 36.2, 31.2, 26.8, 23.6, 22.8, 22.7, 21.7; HRMS [M + H]<sup>+</sup> calculated for C<sub>32</sub>H<sub>42</sub>FeN<sub>4</sub>O<sub>4</sub>, 602.25500, found 602.25488; IR 1636 cm<sup>-1</sup> (Amide I Band); 1511 cm<sup>-1</sup> (Amide II Band); 3293 cm<sup>-1</sup> (Amide A Band).

**Peptide 9.** <sup>1</sup>H NMR (600 MHz, DMSO-*d*<sub>6</sub>)  $\delta$  8.60 (d, 1H, NH Leu, *J* = 8.2 Hz),  $\delta$  8.21 (d, 1H, NH Gly, *J* = 8.2 Hz),  $\delta$  8.11 (t, 1H, NH Fc, *J* = 5.9 Hz),  $\delta$  8.02 (d, 3H, NH Tyr, *J* = 4.1 Hz),  $\delta$  7.16 (d, 2H, ArH, *J* = 8.5 Hz),  $\delta$  6.88 (d, 2H, ArH, *J* = 8.6 Hz),  $\delta$  6.06–6.00 (dtt, 1H, OCH<sub>2</sub>CHCH<sub>2</sub>, *J* = 15.8, 10.4, 5.2 Hz),  $\delta$  5.77–5.69 (m, 1H, CaHCH<sub>2</sub>CHCH<sub>2</sub>),  $\delta$  5.37 (ddd, 1H, OCH<sub>2</sub>CHCHH, *J* = 17.3, 10.3, 1.6 Hz),  $\delta$  5.25 (dd, 1H, OCH<sub>2</sub>CHCHH, *J* = 10.5, 1.4 Hz),  $\delta$  5.08 (dd, 1H, CaHCH<sub>2</sub>CHCHH, *J* = 17.1, 1.4 Hz),  $\delta$  5.00 (d, 1H, CaHCH<sub>2</sub>CHCHH, *J* = 10.2 Hz),  $\delta$  4.53 (d, 2H, OCH<sub>2</sub>CHCH<sub>2</sub>, *J* = 5.2 Hz),  $\delta$  4.46–4.37 (m, 2H, CaH Leu, CaH Gly),  $\delta$  4.19–3.94 (m, 12H, Cp, CaH Tyr, CH<sub>2</sub>Fc),  $\delta$  3.06–3.03 (dd, 1H, CaHCHHPh, *J* = 14.4, 4.7 Hz),  $\delta$  2.86–2.83 (dd, 1H, CaHCHHPh, *J* = 14.4, 8.1 Hz),  $\delta$  2.45–2.30 (m, 2H, CaHCH<sub>2</sub>CHCH<sub>2</sub>),  $\delta$  1.66–1.59 (td, 1H, CH<sub>2</sub>CH(CH<sub>3</sub>)<sub>2</sub>, *J* = 13.5, 6.7 Hz),  $\delta$  1.50–1.45 (m, 2H, CH<sub>2</sub>CH(CH<sub>3</sub>)<sub>2</sub>),  $\delta$  0.90–0.86 (m, 6H, CaHCH<sub>2</sub>CH(CH<sub>3</sub>)<sub>2</sub>); <sup>13</sup>C NMR (150 MHz, DMSO-*d*<sub>6</sub>)  $\delta$  171.1, 170.1, 167.6, 157.3, 134.0, 133.7, 130.6, 126.6, 117.3, 114.6, 85.9, 71.5, 70.9, 70.3, 68.3, 68.1, 67.5, 67.4, 67.3, 67.2, 67.1, 53.2, 52.0, 51.0, 48.5, 41.1, 40.0, 37.4, 36.3, 36.0, 23.9, 22.9, 21.6; HRMS [M + H]<sup>+</sup> calculated for C<sub>34</sub>H<sub>44</sub>FeN<sub>4</sub>O<sub>4</sub>, 628.27065, found 628.26923; IR 1641 cm<sup>-1</sup> (Amide I Band); 1512 cm<sup>-1</sup> (Amide II Band); 3277 cm<sup>-1</sup> (Amide A Band).

**Electrochemistry.** All electrochemical measurements were taken with a CHI 650D electrochemical analyzer (CH Instruments, Inc.) with ohmic-drop correction at room temperature. A peptide modified gold surface formed the working electrode<sup>23</sup> (geometric area of 0.33 cm<sup>2</sup>), with a platinum mesh and Ag/AgCl wire used as the counter and reference electrodes, respectively. The Ag/AgCl reference electrode was calibrated after each experiment against the ferrocene/ferricenium couple. Ferrocene-derivatized peptide electrodes were electrochemically characterized in 0.1 mol L<sup>-1</sup> tetra-*n*-butylammonium hexafluorophosphate (TBAPF<sub>6</sub>)/CH<sub>3</sub>CN solutions. The digitized, background-subtracted curves were analyzed using a Data Master 2003 program.

**Computational Methods.** The lowest energy conformers for all of the *N*-protected peptides were determined in Gaussian 09, with tight convergence criteria using a hybrid B3LYP method with 6-31G\*\* basis set for all C, H, N, O atoms, and LanL2dz basis set for the Fe atom in order to define the backbone conformations of all peptides. The geometry of each diabatic state was optimized using the latest constrained density functional theory (cDFT)<sup>28</sup> as implemented in NWChem 6.1.1<sup>29</sup> using the B3LYP density functional method with 6-31G\*\* basis set for all C, H, N, O atoms, and LanL2dz basis set for the Fe atom. Diabatic potential profiles were determined by assuming that during an electron transfer step the nuclear configuration changes smoothly between the optimized geometries of the diabatic states in which the excess electron is localized before and after electron transfer.<sup>30</sup> Thus, the energy of each of the two diabatic states along the electron transfer reaction coordinate was taken as the energy for geometries linearly interpolated between the optimized geometries of the two diabatic states, with the excess electron localized to the part of the molecule corresponding to the diabatic state in question. In these calculations, the solvent effects were taken into account approximately by the COSMO approach. The Löwdin electron population analysis for uncharged and charged amino acids was conducted by respectively placing the charge of 0 and +1 on the individual residue within the linear helical peptide, namely an Aib or a modified serine with electron rich alkene side-chain, using the B3LYP density functional method with 6-31G\*\* basis set for all C, H, N, O atoms, and LanL2dz basis set for the Fe atom.<sup>7</sup>

## RESULTS AND DISCUSSION

**Peptide Design.** Aib residues were incorporated into peptides 1–6 in order to promote the formation of a unifying 3<sub>10</sub>-helical secondary structure.<sup>23</sup> The peptides 1, 4, 5, and 6 also contain alkenes as potential hopping sites for electron transfer, where this group is part of the macrocycle of 1. The peptides 2 and 3 lack an alkene and hence provide suitable controls. The diene of 6 is positioned in the *i* and *i* + 3 residues, to locate the alkenes on the same side of the molecule in the helix in a proximal arrangement to promote electron transfer. This diene also allows cyclization by ring closing metathesis (RCM) to introduce a covalent tether to further constrain the peptide backbone into a 3<sub>10</sub>-helix and to rigidify the backbone into this geometry. The  $\beta$ -strand constrained peptides (7 and 8) have the covalent tether linking the *i* and *i* + 2 residues. Such a 17-membered ring, with an aryl group at the *N*-terminus is known to stabilize a  $\beta$ -strand geometry with the associated rigidification of the backbone.<sup>27</sup> The linear diene 9 was also prepared as a control for the electrochemical studies.

**Conformational Analysis of Peptides.** The geometry of peptides 1–6 was confirmed as 3<sub>10</sub>-helical by <sup>1</sup>H NMR spectroscopy. In particular, strong NH (*i*) to NH (*i* + 1) ROESY correlations were found for peptides 1–6, together with CaH (*i*) to NH (*i* + 1) and medium range CaH (*i*) to NH (*i* + 2) correlations, as shown in Figure 3 and the Supporting

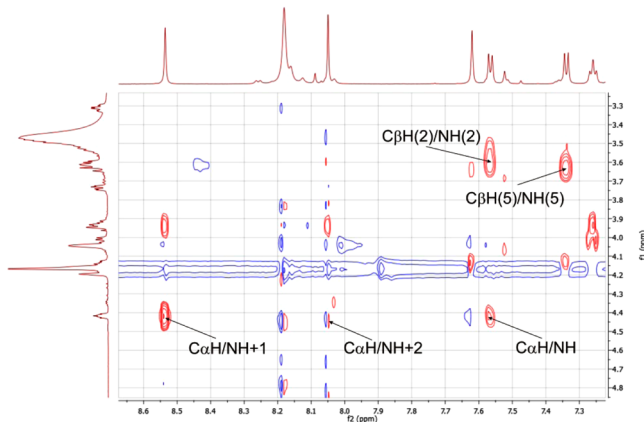


**Figure 3.** <sup>1</sup>H NMR ROESY spectrum representative of peptide 2, showing CaH (*i*) to NH (*i* + 1), CaH (*i*) to NH (*i* + 2) and C $\beta$ H<sub>2</sub> (*i*) and NH (*i*) crosspeaks, indicative of a 3<sub>10</sub>-helical conformation.

Information. A CaH (*i*) to NH (*i* + 2) cross peak is only possible for a 3<sub>10</sub>-helix,<sup>31</sup> as the distance between these two hydrogen atoms is in the order of 3.5 Å, whereas in an  $\alpha$ -helix the distance between CaH (*i*) to NH (*i* + 2) atoms is approximately 4.5 Å, and near the limit of detection.<sup>32</sup> An absence of CaH (*i*) to NH (*i* + 4) correlations was noted for all peptides, thus excluding the possibility of an  $\alpha$ -helical structure, which is characterized by (*i* to *i* + 4) hydrogen bonds.<sup>33</sup> Strong correlations were also evident for C $\beta$ H<sub>2</sub> (*i*) and NH (*i*) in peptides 1 and 2.<sup>34</sup> Hence the cumulative <sup>1</sup>H NMR data confirms the presence of 3<sub>10</sub>-helical structures for each of peptides 1–6.

The conformations of peptides 7–9 were confirmed as  $\beta$ -strand by a combination of <sup>1</sup>H NMR and IR spectroscopy. CaH (*i*) to NH (*i* + 1) and C $\beta$ H (*i*) to NH (*i* + 1) ROESY correlations were found for all three peptides, indicative of a  $\beta$ -strand geometry<sup>35</sup> (see Supporting Information). Furthermore,

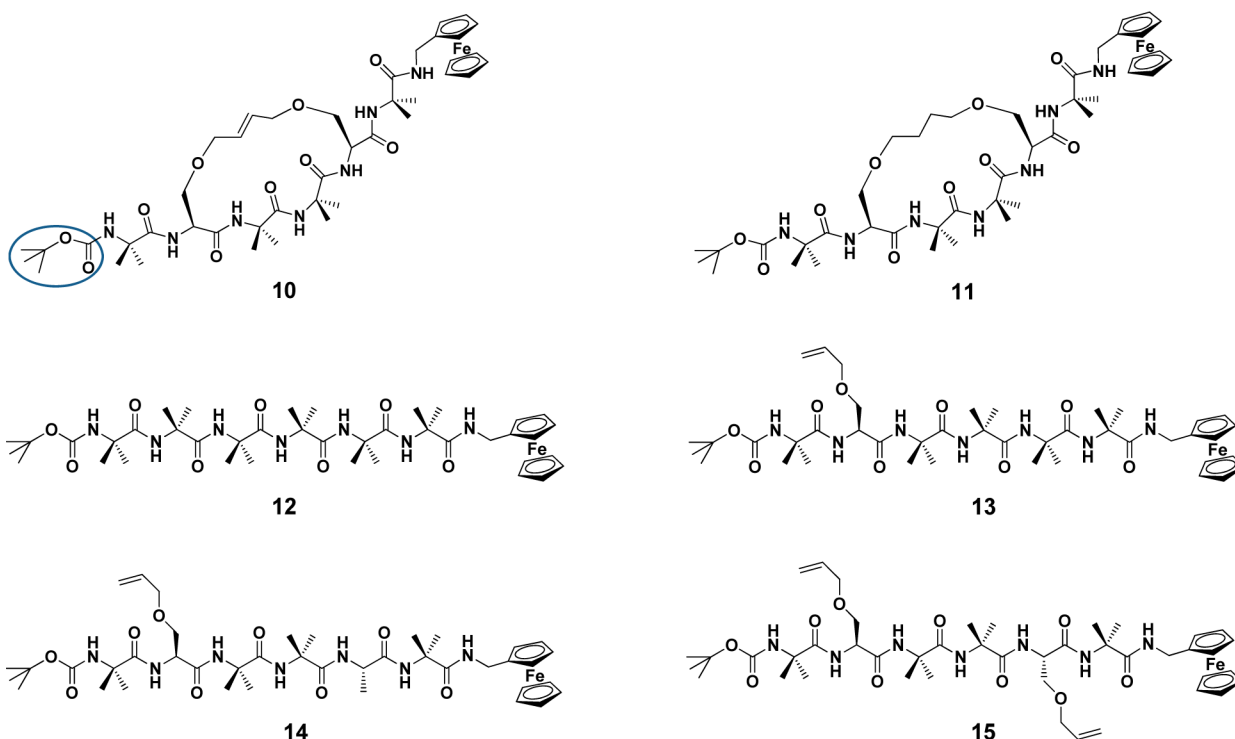


**Figure 4.** Lowest energy conformers for the *N*-protected analogues of 1–6 (peptides 10–15). The *N*-Boc protection group is circled in Peptide 10.

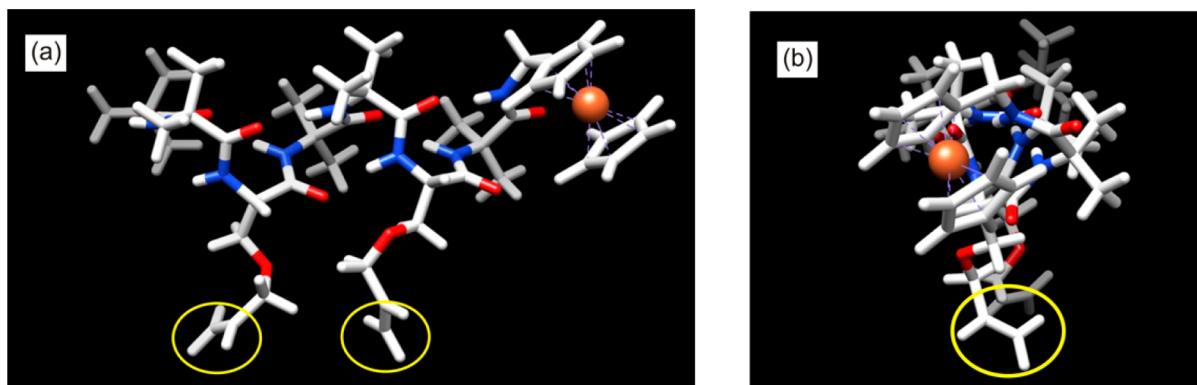


**Figure 5.** (a) The lowest energy conformer for peptide 15 (analogue of 6) showing the two side-chains facing each other in a proximal arrangement (circled) and (b) the view looking down the helix, which indicates that the two side-chains are in the same plane (circled). (Optimized by the hybrid B3LYP method with 6-31G\*\* basis set for all C, H, O, N atoms and Lanl2dz for Fe atom.)

$^1\text{H}$  NMR  $J_{\text{NHC}\alpha\text{H}}$  coupling constants<sup>35</sup> of 8–10 Hz were observed for these peptides. Amide I and II bands, used extensively in peptide/protein structural determination, were found to be in the range assigned to a  $\beta$ -strand conformation<sup>36</sup> for all three tripeptides. Amide A (N–H stretching) frequencies between 3277 and 3293  $\text{cm}^{-1}$  were also observed in the IR spectra of peptides 7–9, indicative of the presence of hydrogen bonding within ordered  $\beta$ -sheets<sup>37</sup> (see Supporting Information).

The lowest energy conformers for the *N*-protected analogues of 1–9 (see peptides 10–18, Figures 4 and 6) were determined by molecular modeling in order to further define the backbone geometries. The *N*-protected peptides were used in these studies, as free amines are known to give rise to unrealistic electrostatic interactions, resulting in unstable lowest energy conformers.<sup>38</sup> The lowest energy conformers for the *N*-protected helical hexapeptides 10–15 (see Figure 4) were

calculated. The resulting models indicate that the backbone lengths (from first to last carbonyl carbons) are almost identical, differing by no more than 0.04 Å. The mean hydrogen bond lengths in the constrained helical peptides 10 and 11 is 2.10 Å, which is in accordance with similar  $3_{10}$ -helical structures,<sup>23,24,34</sup> and 2.12 Å in the unconstrained helical peptides 12–15 (see Supporting Information), also similar to those reported elsewhere.<sup>23,24,34</sup> The most significant difference in the intramolecular hydrogen bond lengths for each of the helical peptides is only 0.15 Å, between residues 2 and 5 in peptides 10 and 15, which correspond to the  $i$  and  $i + 3$  positions of the constraint. The average dihedral angles for residues 1–6 in each of the *N*-Boc protected analogues, deviate from an ideal  $3_{10}$ -helix by no more than 3.6° and 5.9° for  $\Phi$  and  $\psi$ , respectively. Figure 5 shows the lowest energy conformer for 15, revealing that the side-chains are positioned on the same side of the molecule, with the terminal alkenes separated by 6 Å.

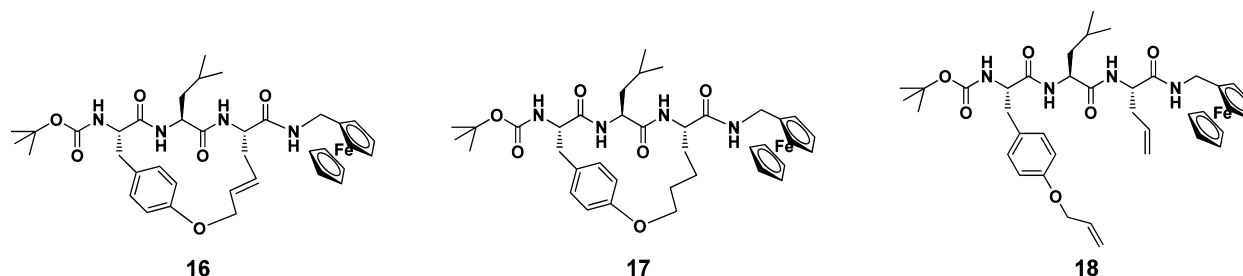


Figure 6. Lowest energy conformers for the *N*-protected analogues of 7–9 (peptides 16–18).

The calculated lowest energy conformers for the *N*-protected  $\beta$ -strand peptides 16, 17 and 18, (see Figure 6) indicate that the backbone length (from first to last carbonyl carbons) are once again almost identical, with the backbone length of the constrained peptides differing by only 0.05 Å. The largest variation in backbone length is 0.30 Å, between the linear analogue (18) and the unsaturated peptide (16). All other dimensions critical to the characterization of a  $\beta$ -strand conformation, such as  $NH(i)$  to  $NH(i+1)$ ,  $CaH(i)$  to  $NH(i+1)$  and  $C\beta H_2(i)$  to  $NH(i+1)$  distances (see Supporting Information) are in accordance with literature values.<sup>39</sup> Figure 7 shows the lowest energy conformers for peptides 16 and 17, highlighting the structural difference between the side-chains of the saturated and unsaturated molecules.

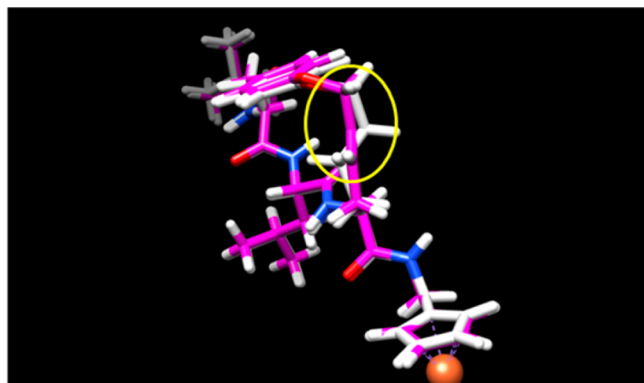


Figure 7. Lowest energy conformers for peptides 16 and 17, analogues of 7 and 8 (overlapped), optimized by the hybrid B3LYP method with 6-31G\*\* basis set for all C, H, O, N atoms and LanL2dz for Fe atom. The side-chain of the unsaturated 16 is depicted in white, with that of peptide 17 in pink. The saturated/unsaturated models overlap fittingly, with the exception of the highlighted region about the double bond.

A combination of the molecular modeling studies and the <sup>1</sup>H NMR and IR data demonstrates that peptides 10–15 share remarkably similar  $3_{10}$ -helical conformations, while peptides 16–18 exhibit a common  $\beta$ -strand geometry. Thus, the prominent structural differences between each of these peptides and hence the analogues (1–6 and 7–9) are simply the variation in the number of electron rich alkenes, the presence (or absence) of the side-bridge constraint, and the associated effect that this has on backbone rigidity as discussed below.

**Electrochemical Analysis of Intramolecular Electron Transfer.** Each of the peptides 1–9 was separately attached to vertically aligned single-walled carbon nanotube array/gold (SWCNTs/Au) electrodes<sup>40</sup> in order to study their electron transfer kinetics. SWCNTs/Au electrodes were used in this

study to provide a high surface concentration of redox probes, with an associated significant increase in sensitivity and reproducibility of the electrochemical measurement over bare Au electrodes.<sup>40</sup> Analysis of the electrochemical results for the helical peptides 1–6 reveal a pair of redox peaks in each cyclic voltammogram, characteristic of a one-electron oxidation/reduction reaction ( $Fc^+/Fc$ ) (see Figure 8). The formal potentials ( $E_0$ ) and apparent electron transfer rate constants ( $k_{app}$ ) were estimated using Laviron's formalism,<sup>41</sup> and given in Table 1.

A comparison of the data for the peptides 1, 4 and 5 provides some insight into the influence of backbone rigidity, where these peptides share a common  $3_{10}$ -helical geometry and the presence of a single alkene. Peptide 1 is constrained and hence rigidified by its tether. Peptide 4 contains five Aib residues, while peptide 5 would be the most flexible of the three with an Ala residue in place of one Aib at the site of cyclization in 1. The data on these compounds reveals an electron transfer rate constant for the macrocyclic peptide 1 of  $17\text{ s}^{-1}$ , a clear 15–20 fold lower than that of peptides 4 and 5. Peptide 4 gave the next lowest electron transfer rate constant ( $260\text{ s}^{-1}$ ), with the most flexible peptide 5 displaying a value of  $307\text{ s}^{-1}$ . Thus, there is a clear correlation between the electron transfer rate constant and the flexibility of the peptide backbone. Increased rigidity impedes electron transfer, presumably by restricting the precise torsional motions required by a hopping mechanism, that lead to facile intramolecular electron transfer along the peptide.<sup>23,42</sup>

A dramatic shift to the positive in the formal potential of the constrained peptide 1, compared to those of the linear analogues 4 and 5, was also observed. The difference between the formal potentials of the constrained (1) and unconstrained (4 and 5) peptides was a significant 465 mV. This is similar to results from our previous study involving a hexapeptide that was also stapled  $i$  to  $i+3$ , but by a triazole containing linker introduced by an alternative Huisgen cycloaddition strategy (480 mV).<sup>23</sup> Such a marked disparity between the formal potentials of these linear and macrocyclic peptides is further evidence of the additional backbone rigidity imparted by the side-bridge constraint. The observed effect on electron transfer is the result of cyclization and the associated rigidification, rather than by the makeup of the component macrocycle.

A comparison of the data for the three linear hexapeptides (3, 4, and 6) provides a measure of the influence of the electron rich alkene side-chains on the rate of electron transfer somewhat in isolation from the effects of backbone rigidity. Peptide 6, with alkenes at both the  $i$  and  $i+3$  positions, exhibited the largest electron transfer rate constant of  $388\text{ s}^{-1}$ . The peptide containing one alkene side chain (4) gave an electron transfer rate constant of  $260\text{ s}^{-1}$ . Peptide 3, which lacks an alkene side chain in its sequence, gave a much reduced

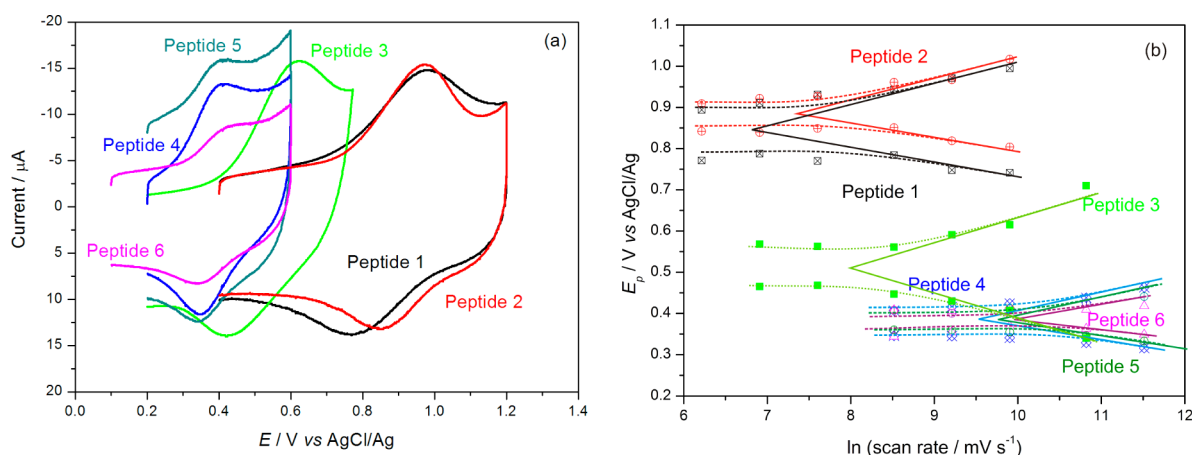


**Figure 8.** (a) Cyclic voltammograms for peptides 1–6 immobilized on SWCNTs/Au electrodes taken at  $5 \text{ V s}^{-1}$ . (b) Peak potential versus  $\ln(\text{scan rate})$  for peptides 1–6 after background current subtraction.

**Table 1. Electron Transfer Rate Constants ( $k_{\text{app}}$ ), Surface Concentrations and Formal Potentials ( $E_0$ ) for the Helical Peptides (1–6)**

peptide	surface concentration ( $\times 10^{-10} \text{ mol cm}^{-2}$ )	$E_0$ (V vs AgCl/Ag)	$k_{\text{app}}/\text{s}^{-1}$
1	$4.37 \pm 0.43$	0.844	$17.49 \pm 1.46$
2	$4.19 \pm 0.35$	0.881	$31.88 \pm 2.82$
3	$9.79 \pm 0.21$	0.508	$62.90 \pm 5.35$
4	$4.02 \pm 0.41$	0.380	$260.38 \pm 25.32$
5	$4.12 \pm 0.48$	0.379	$307.11 \pm 30.61$
6	$3.58 \pm 0.37$	0.375	$388.44 \pm 37.94$

electron transfer rate constant of  $62 \text{ s}^{-1}$ . The electron transfer rate constant clearly increases with the increasing number of electron rich alkenes in the peptides, which presumably facilitate electron transfer, by way of a hopping mechanism utilizing the alkenes as “stepping stones”.

It is important to note that the relative rigidity of the backbones of peptides 3, 4, and 6 may also contribute to the rate of electron transfer, which would be expected to decrease with increasing numbers of Aib units through the series as discussed above and elsewhere.<sup>23</sup> A comparison of the data for peptides 5 and 6 sheds further light on this suggestion. These two peptides contain the same number of Aib units and differ only in the number of alkenyl groups to act as potential “stepping stones”. The observed electron transfer rate constant for 6 was  $388 \text{ s}^{-1}$ , 20% higher compared to that for 5 ( $307 \text{ s}^{-1}$ ). This clearly demonstrates the ability of the alkene groups to facilitate electron transfer through the peptide by acting as a “stepping stone”. It is thus clear that a combination of both the electronic properties and the extent of backbone rigidity determines the rate of electron transfer in peptides.

A comparison of the unsaturated and saturated macrocyclic peptides 1 and 2 provides further insights into the role of these two effects on the efficiency of electron transfer. Unlike the linear peptides 4, 5 and 6, the planar alkene of 1 is able to influence both the backbone rigidity and potentially the electronic properties with its inclusion in a ring. One might expect this alkene to enhance backbone rigidity, while at the same time providing a potential “stepping stone” for electron transfer. These effects are opposing, with the first expected to decrease the electron transfer rate and the second to increase it. Interestingly, the unsaturated macrocycle 1 gave an approximate 2-fold decrease in the electron transfer rate relative to 2,

with values of 17 and  $31 \text{ s}^{-1}$ , respectively. This observation is reinforced for the two  $\beta$ -strand constrained peptides, the unsaturated macrocycle 7 and the saturated analogue 8 which displayed electron transfer rates of 11 and  $23 \text{ s}^{-1}$ , respectively (see Tables 1 and 2). Clearly, increasing backbone rigidity in

**Table 2. Electron Transfer Rate Constants ( $k_{\text{app}}$ ), Surface Concentrations and Formal Potentials ( $E_0$ ) for the  $\beta$ -Strand Peptides (7–9)**

peptide	surface concentration ( $\times 10^{-10} \text{ mol cm}^{-2}$ )	$E_0$ (V vs AgCl/Ag)	$k_{\text{app}}/\text{s}^{-1}$
7	$9.21 \pm 0.89$	0.676	$11.72 \pm 1.16$
8	$7.13 \pm 0.68$	0.827	$23.62 \pm 2.13$
9	$5.56 \pm 0.31$	0.408	$421.36 \pm 41.51$

both secondary structures ( $3_{10}$ -helix and  $\beta$ -strand) decreases the efficiency of electron transfer. Curiously, the saturated helical peptide 2 exhibited a formal potential shift to the positive of 37 mV compared to the unsaturated analogue 1. The saturated  $\beta$ -strand peptide 8 recorded an even greater formal potential shift to the positive of 151 mV relative to its unsaturated analogue 7 (see Figure 9). Thus, oxidation/reduction of the ferrocene moiety in both of the saturated peptides is energetically less favorable than in the corresponding unsaturated peptides. However, the observed electron transfer rate constants for both saturated peptides are almost double that of their unsaturated counterparts. As noted here for 1, 2, 7, 8, and elsewhere,<sup>23</sup> peptides constrained by a side-chain tether give rise to a significant increase in the formal potentials relative to their linear analogues, reflecting the associated increase in backbone rigidity. Thus, any formal potential shift to the positive is usually combined with a reduction in the electron transfer rate constant. Therefore, while the effect of backbone rigidity appears to be the dominant factor in this case, it would also be expected that the electron rich alkene in the tether of peptides 1 and 7 should enhance electronic coupling. However, further investigation is required to substantiate this notion, and this is developed further in the following computational study section.

**Computational Study on Intramolecular Electron Transfer.** High level theoretical calculations, using the latest constrained density functional theory (cDFT), were conducted on  $\beta$ -strand models 19, 20, and 21 in order to provide further

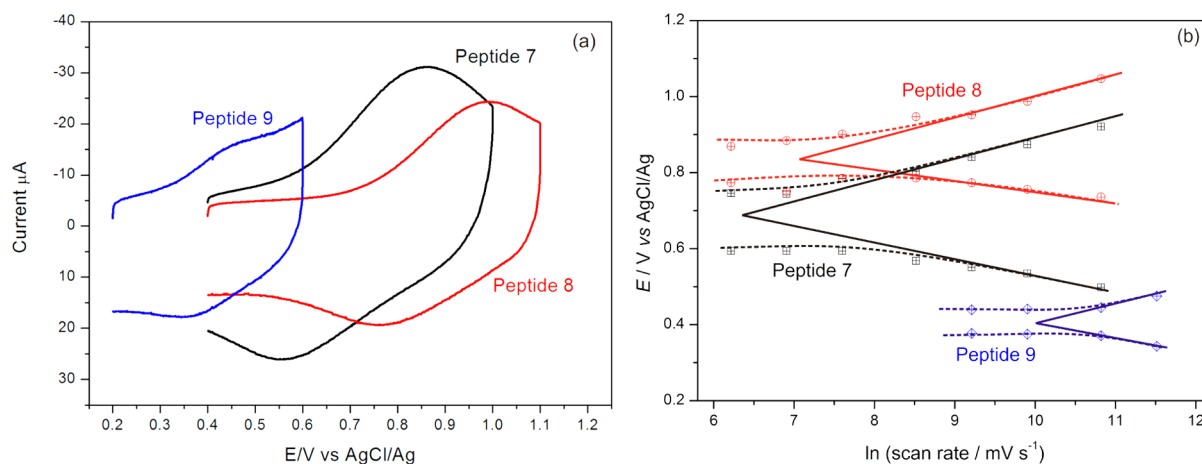


**Figure 9.** (a) Cyclic voltammograms for  $\beta$ -strand peptides 7–9 immobilized on SWCNTs/Au electrodes taken at 5 V s<sup>-1</sup>. (b) Peak potential versus ln (scan rate) for peptides 7–9 after background current subtraction.

insights into the relative roles of backbone rigidity and electron rich side-chains on intramolecular electron transfer (see Figure 10). These peptides are analogous to 7, 8 and 9, but with

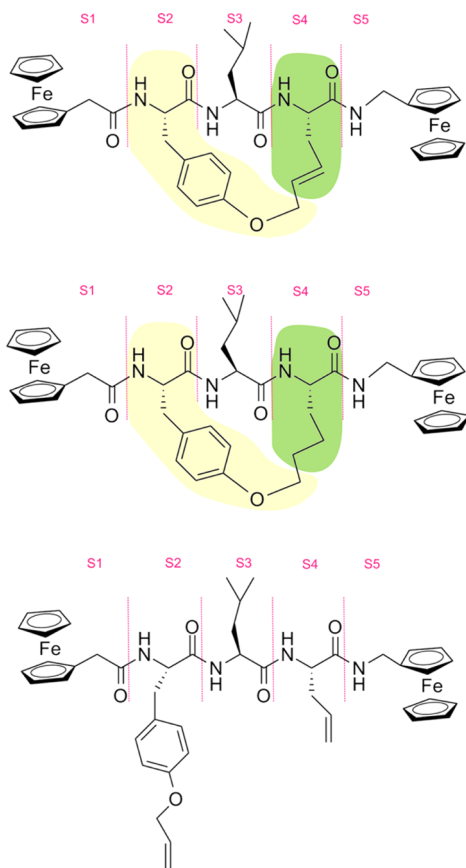


**Figure 10.** Constructed diabatic states in model peptides 19 (top), 20 (middle) and 21 (bottom).

ferrocene units included at both termini to act as both donor and acceptor. Diabatic states were constructed by individually localizing an overall charge of +1 on each of the amino acids and ferrocene units,<sup>28</sup> as shown in Figure 10. Reorganization energies ( $\lambda$ ) for electron transfer along the backbone were calculated, together with electronic coupling constants ( $H_{ab}$ ) in

order to provide an insight into the overall intramolecular electron transfer dynamics.

A trend between the electronic coupling constants ( $H_{ab}$ ) and the number of double bonds in each side-chain is evident. The structure with the greatest number of electron rich side-chains (unconstrained peptide 21) has the largest coupling constant (0.106 eV). This is sequentially followed by the unsaturated peptide 19 (0.087 eV), and the saturated peptide 20 (0.049 eV) (see Table 3). Significantly, the electronic coupling constant for

**Table 3.** Electronic Coupling Constants ( $H_{ab}$ ), the Number of Double Bonds in Each Side-Chain and Average Reorganization Energies ( $\lambda$ ) for Peptides 19–21, and the Formal Potentials ( $E_o$ ) and Electron Transfer Rate Constants ( $k_{app}$ ) for Their Analogues, Peptides 7–9

peptide	formal potential ( $E_o$ ) (V vs AgCl/Ag)	$H_{ab}$ (eV)	number of C=C in side chains	average reorganization energy ( $\lambda$ ) (eV)	$k_{app}/s$
20 (8)	0.827	0.049	0	0.65	23
19 (7)	0.676	0.087	1	0.74	11
21 (9)	0.408	0.106	2	0.35	421

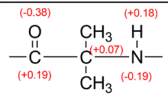
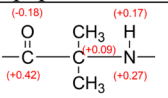
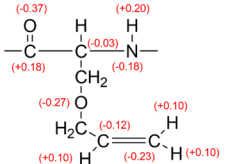
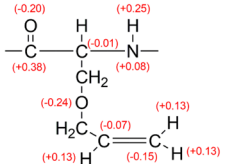
unsaturated 19 (0.087 eV) is almost double that of the saturated analogue 20 (0.049 eV). This clearly indicates that the electron rich alkene in the tether of the unsaturated peptide does indeed enhance electronic coupling.

Furthermore, the formal potential observed experimentally for the unsaturated peptide 7 is significantly lower than that observed for the saturated 8 (see Table 3). This lower potential is clearly attributable to the effect of the electron rich  $\pi$ -bond in the side-chain of 7. In contrast, the higher reorganization energy calculated for the derivative of 7 (unsaturated analogue 19 (0.74 eV)), relative to the derivative of 8 (saturated analogue 20 (0.65 eV)), is likely the direct consequence of the lack of rotational freedom available in the side-chain of the unsaturated peptide. This leads to an increase in the rigidity of the backbone and consequently to the lower rate of electron transfer observed for unsaturated 7, compared to saturated 8.

Additionally, a large difference of up to 0.49 eV is apparent between the reorganization energies of the constrained peptides



Table 4. Löwdin Analysis of the Charge Distribution on Uncharged and Charged Amino Acid Residues (1) Aib and (2) Modified Serine with Electron Rich Alkene Side-Chain

	Uncharged peptide unit	With overall charge of +1 localized on single peptide unit	The extra charge localized in amide bonding region	The extra charge localized in CH=CH <sub>2</sub> region
(1) Aib			0.88	
(2) Modified serine with electron rich alkene side-chain			0.68	0.22

(19 and 20), and those of the unconstrained 21 (see Table S13, Supporting Information). The unconstrained peptide 21 gave rise to the highest calculated ( $H_{ab}$ ) and the lowest calculated ( $\lambda$ ) based on Marcus theory,<sup>43</sup> which suggests that oxidation/reduction of the ferrocene moiety is energetically more favorable in the linear peptide, than in either of the constrained compounds. This supports the earlier experimental observation where the linear peptide 9 exhibited the lowest formal potential relative to the two constrained peptides 7 and 8 (by between 268 and 419 mV), and the highest electron transfer rate constant (an 18–38 fold increase) relative to 7 and 8 (see Table 3). This is indicative of the additional backbone rigidity imparted by the constraint. Thus, the influence of the electron rich alkenes and any effects arising from a change in backbone rigidity can be studied in isolation using a combination of experimental and theoretical studies. Both factors clearly contribute to the rate of electron transfer in peptides.

Electron population analysis (EPA) was conducted to further elucidate the role of electron rich side-chains as “stepping stones” for electron transfer. The amino acid residues used in the synthesis of the linear helical peptides (4, 5 and 6), namely, an Aib and a modified serine with electron rich alkene side-chain were considered. A Löwdin analysis of the charge distribution from the cDFT calculations on the charged and uncharged amino acid residues is shown in Table 4. Approximately 88% of the extra charge is distributed on the amide region when the positive charge (+1) was injected into the Aib residue. This emphasizes the significant contribution made by the amide region to intramolecular electron transfer through the peptide backbone, clearly demonstrating the participation of a through-bond hopping mechanism.<sup>7</sup> However, when the positive charge (+1) was injected into the modified serine residue, only 68% of the extra charge was distributed on the amide region, with the electron rich alkene side-chain holding approximately 20% of the extra charge localized on the residue (see Table 4). Thus, these results confirm the role of the electron rich alkene side-chain as a “stepping stone” for electron transfer.

## CONCLUSION

Electrochemical studies are reported on a series of peptides (1–9) in order to elucidate the effect of backbone rigidity and the nature of the amino acid side chains in defining the rate of electron transfer. Aib residues were incorporated into peptides 1–6 to promote the formation of a unifying 3<sub>10</sub>-helical secondary structure, with the number of alkenes in their side-

chains varying from 0 to 2. The backbones of peptides 1 and 2 were further constrained into a 3<sub>10</sub>-helix with a side chain tether introduced by RCM. The side-chain of 1 contains a single C=C double bond, while peptide 2 is fully saturated. Peptides 7–9 share a common  $\beta$ -strand conformation, with 7 (unsaturated) and 8 (saturated) further rigidified into this geometry via cyclization by RCM. Electrochemical studies conducted on peptides 1, 4 and 5, each containing a single alkene in their structure, revealed a direct link between backbone rigidity and the efficiency of electron transfer. The significant difference in the formal potentials of the constrained 1 and unconstrained 4 and 5, (465 mV) is in accordance with our previous study (480 mV).<sup>23</sup> This demonstrates a general observation, where a tether hinders electron transfer in peptides by restricting backbone flexibility. Further studies on the linear peptides 3–6, containing between 0 and 2 electron rich side-chains in their structure, confirmed the ability of the alkene to facilitate electron transfer through the peptide, while nullifying the effects of backbone rigidity.

The macrocyclic helical peptides reveal a formal potential shift to the positive and subsequent reduction of the electron transfer rate constant for unsaturated 1, relative to saturated 2. Comparable results were also evident for the unsaturated (7) and saturated (8)  $\beta$ -strand peptides.

The only structural difference between the unsaturated and saturated peptides is the presence or otherwise of the electron rich  $\pi$ -bond in the side-chain, so the lower the electron transfer rate constants observed for both unsaturated peptides (1 and 7) are likely a direct consequence of the lack of rotational freedom about this double bond, which results in further rigidification of the peptide backbone. High level calculations performed on peptides 19 and 20 (analogues of 7 and 8) confirmed that the reorganization energy is greater in the unsaturated peptide (19), thus supporting the observed lower electron transfer rate constant of 7, relative to saturated 8. However, the lower formal potential observed experimentally for the unsaturated 7, suggests that oxidation/reduction of the ferrocene moiety is energetically more favorable in 7. Theoretical calculations show that the derivative of the unsaturated peptide 7 (19), exhibited a higher electronic coupling constant than its saturated counterpart 20, which helps to explain this paradox, while further demonstrating the ability of the alkene to facilitate electron transfer. Thus, the theoretical electronic coupling constants and reorganization energies, together with the formal potentials and electron transfer rate constants observed experimentally for the

macrocyclic peptides, reveal for the first time an interplay between electron rich alkene side-chains and backbone rigidity, with both factors clearly shown to contribute to the efficiency of electron transfer in peptides. Additional high level calculations were also performed on the amino acid residues used in the synthesis of the linear helical peptides (4, 5 and 6), namely, an Aib and a modified serine with electron rich alkene side-chain. Injection of a positive charge into the modified serine residue shows that approximately 20% of the extra charge is localized on the electron rich side-chain, so confirming the role of the alkene as a “stepping stone” for electron transfer.

These findings provide a new approach to fine-tune the electronic properties of peptides through chemical modification of the backbone to increase/decrease rigidity, and through the inclusion of electron rich side-chains. Such structurally diverse peptides with controllable electronic functions open new avenues in the design and fabrication of efficient components for molecular-based electronic devices.

## ■ ASSOCIATED CONTENT

### ■ Supporting Information

Synthesis of peptides, ROESY spectra of peptides 1, 4, 5, 6, 7, 8 and 9, IR spectra for peptides 7–9, computational models of peptides 10, 11, 13, 14, 15, 16, 17 and 18, electrochemical measurements, diabatic potential profiles and reorganization energies in the three model peptides 19, 20 and 21, <sup>1</sup>H NMR spectra for target peptides and their key synthetic intermediates. This material is available free of charge via the Internet at <http://pubs.acs.org>.

## ■ AUTHOR INFORMATION

### Corresponding Authors

jingxian.yu@adelaide.edu.au  
andrew.abell@adelaide.edu.au

### Notes

The authors declare no competing financial interest.

## ■ ACKNOWLEDGMENTS

We would like to thank Miss Kyra Middlemiss for her assistance with the synthesis of helical peptide precursors. The financial support of this work by the Australian Research Council is gratefully acknowledged. The computational aspects of this work were supported by an award under the National Computational Merit Allocation Scheme for J.Y. on the National Computing Infrastructure (NCI) National Facility at the Australian National University.

## ■ REFERENCES

- (1) Isied, S. S.; Ogawa, M. Y.; Wishart, J. F. *Chem. Rev.* **1992**, *92*, 381.
- (2) Ron, I.; Sepunaru, L.; Itzhakov, S.; Belenkova, T.; Friedman, N.; Pecht, I.; Sheves, M.; Cahen, D. *J. Am. Chem. Soc.* **2010**, *132*, 4131.
- (3) Yu, J.; Zvarec, O.; Huang, D. M.; Bissett, M. A.; Scanlon, D. B.; Shapter, J. G.; Abell, A. D. *Chem. Commun.* **2012**, *48*, 1132.
- (4) Mandal, H. S.; Kraatz, H.-B. *J. Phys. Chem. Lett.* **2012**, *3*, 709.
- (5) Malak, R. A.; Gao, Z. N.; Wishart, J. F.; Isied, S. S. *J. Am. Chem. Soc.* **2004**, *126*, 13888.
- (6) Yu, J.; Horsley, J. R.; Abell, A. D. *Aust. J. Chem.* **2013**, *66*, 848.
- (7) Yu, J.; Huang, D. M.; Shapter, J. G.; Abell, A. D. *J. Phys. Chem. C* **2012**, *116*, 26608.
- (8) Chaudhry, B. R.; Wilton-Ely, J.; Tabor, A. B.; Caruana, D. J. *Phys. Chem. Chem. Phys.* **2010**, *12*, 9996.
- (9) Lauz, M.; Eckhardt, S.; Fromm, K. M.; Giese, B. *Phys. Chem. Chem. Phys.* **2012**, *14*, 13785.

- (10) Yasutomi, S.; Morita, T.; Imanishi, Y.; Kimura, S. *Science* **2004**, *304*, 1944.
- (11) Cordes, M.; Kottgen, A.; Jasper, C.; Jacques, O.; Boudebous, H.; Giese, B. *Angew. Chem., Int. Ed.* **2008**, *47*, 3461.
- (12) Gao, J.; Mueller, P.; Wang, M.; Eckhardt, S.; Lauz, M.; Fromm, K. M.; Giese, B. *Angew. Chem., Int. Ed.* **2011**, *50*, 1926.
- (13) Wang, M.; Gao, J.; Muller, P.; Giese, B. *Angew. Chem., Int. Ed.* **2009**, *48*, 4232.
- (14) Watanabe, J.; Morita, T.; Kimura, S. *J. Phys. Chem. B* **2005**, *109*, 14416.
- (15) Long, Y. T.; Abu-Rhayem, E.; Kraatz, H. B. *Chem.—Eur. J.* **2005**, *11*, 5186.
- (16) Wenger, O. S. *Acc. Chem. Res.* **2011**, *44*, 25.
- (17) Polo, F.; Antonello, S.; Formaggio, F.; Toniolo, C.; Maran, F. *J. Am. Chem. Soc.* **2005**, *127*, 492.
- (18) Giese, B.; Graber, M.; Cordes, M. *Curr. Opin. Chem. Biol.* **2008**, *12*, 755.
- (19) Cordes, M.; Giese, B. *Chem. Soc. Rev.* **2009**, *38*, 892.
- (20) Yanagisawa, K.; Morita, T.; Kimura, S. *J. Am. Chem. Soc.* **2004**, *126*, 12780.
- (21) Shih, C.; Museth, A. K.; Abrahamsson, M.; Blanco-Rodriguez, A. M.; Di Bilio, A. J.; Sudhamsu, J.; Crane, B. R.; Ronayne, K. L.; Towrie, M.; Vlcek, A.; Richards, J. H.; Winkler, J. R.; Gray, H. B. *Science* **2008**, *320*, 1760.
- (22) Wittekindt, C.; Schwarz, M.; Friedrich, T.; Koslowski, T. *J. Am. Chem. Soc.* **2009**, *131*, 8134.
- (23) Yu, J.; Horsley, J. R.; Moore, K. E.; Shapter, J. G.; Abell, A. D. *Chem. Commun.* **2014**, *50*, 1652.
- (24) Boal, A. K.; Guryanov, L.; Moretto, A.; Crisma, M.; Lanni, E. L.; Toniolo, C.; Grubbs, R. H.; O’Leary, D. J. *J. Am. Chem. Soc.* **2007**, *129*, 6986.
- (25) Beer, P. D.; Smith, D. K. *J. Chem. Soc., Dalton Trans.* **1998**, 417.
- (26) Ossola, F.; Tomasin, P.; Benetollo, F.; Foresti, E.; Vigato, P. A. *Inorg. Chim. Acta* **2003**, *353*, 292.
- (27) Abell, A. D.; Alexander, N. A.; Aitken, S. G.; Chen, H.; Coxon, J. M.; Jones, M. A.; McNabb, S. B.; Muscroft-Taylor, A. *J. Org. Chem.* **2009**, *74*, 4354.
- (28) Ding, F. Z.; Wang, H. B.; Wu, Q.; Van Voorhis, T.; Chen, S. W.; Konopelski, J. P. *J. Phys. Chem. A* **2010**, *114*, 6039.
- (29) Valiev, M.; Bylaska, E. J.; Govind, N.; Kowalski, K.; Straatsma, T. P.; van Dam, H. J. J.; Wang, D.; Nieplocha, J.; Apra, E.; Windus, T. L.; de Jong, W. A. *Comput. Phys. Commun.* **2010**, *181*, 1477.
- (30) Farazdel, A.; Dupuis, M.; Clementi, E.; Aviram, A. *J. Am. Chem. Soc.* **1990**, *112*, 4206.
- (31) Blackwell, H. E.; Sadowsky, J. D.; Howard, R. J.; Sampson, J. N.; Chao, J. A.; Steinmetz, W. E.; O’Leary, D. J.; Grubbs, R. H. *J. Org. Chem.* **2001**, *66*, 5291.
- (32) Wüthrich, K. *NMR of Proteins and Nucleic Acids*; Wiley: New York, 1986.
- (33) Biron, Z.; Khare, S.; Samson, A. O.; Hayek, Y.; Naider, F.; Anglister, J. *Biochemistry* **2002**, *41*, 12687.
- (34) Jacobsen, O.; Maekawa, H.; Ge, N. H.; Gorbitz, C. H.; Rongved, P.; Ottersen, O. P.; Amiry-Moghaddam, M.; Klaveness, J. *J. Org. Chem.* **2011**, *76*, 1228.
- (35) Pehere, A. D.; Abell, A. D. *Org. Lett.* **2012**, *14*, 1330.
- (36) Zhuang, W.; Hayashi, T.; Mukamel, S. *Angew. Chem., Int. Ed.* **2009**, *48*, 3750.
- (37) Pehere, A. D.; Sumbly, C. J.; Abell, A. D. *Org. Biomol. Chem.* **2013**, *11*, 425.
- (38) Burton, N. A.; Harrison, M. J.; Hart, J. C.; Hillier, I. H.; Sheppard, D. W. *Faraday Discuss.* **1998**, *110*, 463.
- (39) Gillespie, P.; Cicariello, J.; Olson, G. L. *Pept. Sci.* **1997**, *43*, 191.
- (40) Gooding, J. J.; Wibowo, R.; Liu, J. Q.; Yang, W. R.; Losic, D.; Orbons, S.; Mearns, F. J.; Shapter, J. G.; Hibbert, D. B. *J. Am. Chem. Soc.* **2003**, *125*, 9006.
- (41) Laviron, E. *J. Electroanal. Chem.* **1979**, *100*, 263.
- (42) Schlag, E. W.; Sheu, S. Y.; Yang, D. Y.; Selzle, H. L.; Lin, S. H. *Angew. Chem., Int. Ed.* **2007**, *46*, 3196.
- (43) Marcus, R. A.; Sutin, N. *Biochim. Biophys. Acta* **1985**, *811*, 265.